Paper

SELECTIVE SHIELDING OF BONE MARROW: AN APPROACH TO PROTECTING HUMANS FROM EXTERNAL GAMMA RADIATION

Gideon Waterman,* Kenneth Kase,* Itzhak Orion,† Andrey Broisman,* and Oren Milstein*

Abstract—**The current feasibility of protecting emergency responders through bone marrow selective shielding is highlighted in the recent OECD/NEA report on severe accident management. Until recently, there was no effective personal protection from externally penetrating gamma radiation. In Chernobyl, first-responders wore makeshift lead sheeting, whereas in Fukushima protective equipment from gamma radiation was not available. Older protective solutions that use thin layers of shielding over large body surfaces are ineffective for energetic gamma radiation. Acute exposures may result in Acute Radiation Syndrome where the survival-limiting factor up to 10 Gy uniform, homogeneous exposure is irreversible bone marrow damage. Protracted, lower exposures may result in malignancies of which bone marrow is especially susceptible, being compounded by leukemia's short latency time. This highlights the importance of shielding bone marrow for preventing both deterministic and stochastic effects. Due to the extraordinary regenerative potential of hematopoietic stem cells, to effectively prevent the deterministic effects of bone marrow exposure, it is sufficient to protect only a small fraction of this tissue. This biological principle allows for a new class of equipment providing unprecedented attenuation of radiation to select marrow-rich regions, deferring the hematopoietic sub-syndrome of Acute Radiation Syndrome to much higher doses. As approximately half of the body's active bone marrow resides within the pelvis region, shielding this area holds great promise for preventing the deterministic effects of bone marrow exposure and concomitantly reducing stochastic effects. The efficacy of a device that selectively shields this region and other radiosensitive organs in the abdominal area is shown here.**
Health Phys. 113(3):195–208; 2017

Key words: accidents, nuclear; bone marrow; gamma radiation; shielding

INTRODUCTION

The biological effects of ionizing radiation exposure are categorized as stochastic or deterministic. Stochastic effects describe the probability of radiation-induced cancer and/or hereditary defects where increased exposure corresponds to a higher probability of the effects with some latent onset time. Deterministic effects are thought to occur beyond a certain dose threshold and increase in severity with increasing dose. Acute exposure can lead to Acute Radiation Syndrome (ARS). Usually, cells are able to repair the damage in cases where low doses are received. At higher levels of radiation, apoptosis results, and cells that are lost as part of normal tissue turnover are not replaced because of damage to the stem-cell compartment, leading to tissue failure (Stone et al. 2003). Many casualties of the Hiroshima and Nagasaki atomic bombs, and many of the firefighters who first responded to the Chernobyl nuclear power plant accident, became ill with ARS (CDC 2012). The probability of survival of those inflicted with ARS decreases with escalating radiation dose. Most of the people who do not recover from ARS will die within a few weeks to a few months after exposure, with the primary cause of death being the destruction of the body's bone marrow (BM) (CDC 2012). This is exemplified by the Chernobyl firefighters, the majority of whom received whole body doses between 0.8 and 10 Gy, and the United Nations Scientific Committee on the Effects of Atomic Radiation (UNSCEAR) final report on the disaster concluded that the underlying cause of death of all 28 firefighters who succumbed to ARS was from bone marrow failure (UNSCEAR 2000, 2008).

BM is comprised of hematopoietic stem cells (HSCs), which are responsible for the constant renewal of blood cells (Wang and Wagers 2011). Due to their high rate of proliferation, HSCs are especially vulnerable to ionizing radiation but are endowed with remarkable regenerative potential (Dainiak 2002; Greenberger and Epperly 2009; Pearce et al. 1952; Valentine et al. 1952; Valentine and Pearce 1952). Owing to their central role in blood production, lethal irradiation of HSCs leads to death from severe anemia, infection, and internal bleeding. This relationship between high doses of radiation and HSC apoptosis has led to the use of HSC

*Department of Research & Development, StemRad, Ltd., 6 Raoul Wallenberg St. 1st Floor Tel Aviv 6971905, Israel; †Department of Nuclear Engineering, Ben-Gurion University of the Negev. P.O.B. 653, Beer-Sheva 84105, Israel.

The authors declare no conflicts of interest.

For correspondence contact: Oren Milstein, Department of Research & Development, StemRad, Ltd., 6 Raoul Wallenberg St., Tel Aviv 6971905, or email at Israel **oren@stemrad.com**.

(*Manuscript accepted* 29 *March* 2017)
0017-9078/17/0

DOI: 10.1097/HP.0000000000000688

transplantation as a life-saving intervention in cases of acute exposure (Alpen and Baum 1958; Chertkov et al. 1971; Department of Homeland Security 2006; MacVittie 1997; Thomas et al. 1982).

The recovery value of bone marrow is demonstrable in medical practice, where thousands of individuals have undergone supra-lethal Total Body Irradiation (TBI) for purposes of cancer therapy and were rescued by well-matched BM transplantation (Goldman et al. 1986; Thomas et al. 1982). Indeed, life-threatening damage may be reversed by BM transplantation in individuals receiving doses of radiation of up to 10 Gy (Weinstock et al. 2008). At doses > 10 Gy, damage to gastrointestinal (GI) tissue may become a limiting factor in survival (CDC 2012; Barnett et al. 2006). Remarkably, in the common procedure of BM transplantation, the number of HSCs extracted from a single active BM site containing less than 5% of the donor's BM tissue is sufficient to support the complete reconstitution of the HSC compartment in a lethally irradiated recipient (Thomas et al. 1975a and b). This capacity of BM to expand and replenish is due to the high regenerative potential of the HSCs it harbors.

However, allogeneic HSC transplantation has many challenges, especially in large-scale accidents. If mismatched bone marrow transplantation is attempted, graft rejection is likely to ensue (Beatty et al. 1985). There is also a high likelihood of Graft vs. Host Disease (GVHD) (Beatty et al. 1985), an often-fatal condition resulting from an assault of the donor immune cells embedded in the graft on the recipient's bodily tissues. Unfortunately, matched donors are a scarcity due to the tremendous polymorphism in the human leukocyte antigen locus (Hansen et al. 2008). Moreover, transplantation must take place in the immediate days following exposure to radiation, further increasing the challenge in locating a matched donor. In the event of a catastrophe with a large number of victims, the time-frame imposed is not likely to enable isolation of matched donors.

In contrast to mature blood cells, which are dispersed throughout the body, HSCs are confined to the bones, allowing for effective targeted shielding. This has been confirmed in several animal models, where sparing the HSC-rich area of a subject receiving otherwise full-body irradiation is sufficient to support hematopoietic functions and allow survival (Cole et al. 1967; Bertho et al. 2005a and b; Jacobson et al. 1951; MacVittie et al. 2015; Monroy et al. 1988; Stearner et al. 1954; van Bekkum and Schotman 1974). Some of these studies spared approximately 4.5–5% of the non-human primates' BM to mimic heterogeneous exposure conditions to allow for a sufficient number of HSC to remain viable to be subsequently stimulated by granulocyte-colony stimulating factor (G-CSF) therapy (Bertho et al. 2005a; MacVittie et al. 2015; Monroy et al. 1988). Approximately 48% of the human body's active BM is contained within the lumbar vertebrae and the pelvic region (ICRP 2002). This high concentration of BM makes the pelvic region an ideal area to shield for preventing the serious hematopoietic effects of radiation exposure.

Stem-cell rich tissues like active BM are also more sensitive to the stochastic effects (i.e., cancer) of radiation exposure. The high amount of BM in the pelvic region, combined with the presence of the sensitive gastrointestinal system and female gonads in this same area of the body, allows for the possibility of significantly reducing stochastic effects of radiation by limiting radiation exposure to this vital area. Thus, shielding this region holds great promise for both acute and protracted exposures.

Older protective solutions that use thin layers of shielding material over large surfaces of the body create a burden on the wearer; yet at the same time, they are ineffective at blocking energetic gamma radiation. A 2015 Organisation for Economic Co-operation and Development–Nuclear Energy Agency (OECD/NEA) report, Occupational Radiation Protection in Severe Accident Management, states that, "While whole body shielding is inherently heavy, partial body shielding is lighter in weight and selectively shields tissues of increased radiosensitivity (i.e., bone marrow) with substantial amounts of shielding material to protect hematopoietic functions; therefore, potentially preventing the acute health effects of exposure to gamma radiation (i.e., Acute Radiation Syndrome—ARS)" (OECD/NEA 2015).

Thus, a specialized radiation shielding device for the protection of active BM concentrations against gamma radiation is presented here for the first time. This belt-like selective shielding device focuses on the protection of BM that is present in the pelvis and hip bones, protecting the medullary volume from which BM is commonly extracted for transplantation (i.e., the iliac bones) (Thomas et al. 1975a and b) while allowing relatively unhindered movement by the wearer. In order to optimize the use of shielding materials toward the protection of active BM, the shielding uniquely brings into account the natural shielding properties of human tissue, with thickness being inversely related to the thickness and radiation attenuation of the underlying tissue at each point surrounding the area being protected. This selective shielding device is patent-pending under application number US 13/676,995, Radiation protection device and methods (Milstein et al. 2012). The findings resulting from both experimental and simulation testing of this selective shielding device are presented here.

MATERIALS AND METHODS

Engineering of the active bone marrow shield

First, the ideal target for protection was identified. HSCs are present in several BM locations in the human body, the foremost being the pelvis, sternum, ribs, vertebrae, and

skull. In adults, the iliac bones of the pelvis are the most attractive targets for protection due to a high content of active BM (225 g), the iliac bones' relatively small surface area to volume ratio, and the positioning of the iliac bones in the pelvic girdle at the body's center of gravity - an ideal anatomical location for weight-bearing purposes (Watchman et al. 2007). The iliac bones serving as the source of HSCs in BM transplantation validates this choice (Thomas et al. 1975a and b).

Since, depending on recipient weight, between 23 and 58 cm^3, 24–61 g (density of 1.06 g cm^{-3}) (White et al. 1987), of net active BM is harvested and transplanted on average (after deduction of plasma and blood cell infiltrates) (National Marrow Donor Program 1993; Pichardo et al. 2007), the selective shielding device was developed so that a mass of active BM corresponding to this volume will remain viable at least up to a radiation dose where tissues other than BM sustain major damage. The second most radiosensitive tissue is the gut (CDC 2012), and the gut sustains irreversible damage at about 11 Gy (CDC 2012); therefore, the shield was engineered to protect this critical volume of active BM at doses as high as 11 Gy (radionuclide energy dependent), a level that covers most nuclear catastrophes.

In nuclear disasters, radioactive materials are presented in the form of nuclear fallout in a cloud geometry. This dictates that the shield be able to attenuate radiation emanating from all directions, so it is engineered with a circumferential arrangement. The selective shielding device is designed to closely wrap around the area of the body containing the BM selected for protection. Additionally, the selective shielding device covers body surfaces, which are adjacent to the protected BM in order to sufficiently attenuate any radiation approaching the BM through the body of the wearer. To engineer a shield of a weight and design that does not limit mobility, an approach was necessary that would minimize shield mass without compromising protection. Selectively shielding the iliac bones provided an effective means of dramatically reducing shield weight compared to non-selective strategies, but the optimal shield would incorporate into its design the attenuation of the underlying tissue. Also, different tissues (bone > muscle > adipose) have different radiation attenuation. This shield accounts for the natural shielding properties of human tissue by being of differential thickness inversely related to the thickness and radiodensity of the underlying tissue at each point surrounding the target for protection. Thus, at any given point on the selective shielding device, the radiation attenuation factor is such that it accommodates the variation in tissue thickness and radiation attenuation in the circumference of the protected BM, reducing shield mass substantially without compromising protection.

Desired Total Attenuation (A_D) was defined such that the surviving volume of viable active BM is sufficient to allow for hematopoietic reconstitution after exposure. Using previous estimates of the radiosensitivity of human HSCs and progenitors and the volume of active BM that is protected by the selective shielding device, eqn (1) is used to deduce A_D (Senn and McCulloch 1970; Van Bekkum 1991):

$$A_D \geq \frac{D_U}{D_V} \tag{1}$$

$$P_R = \frac{V_N}{V_P} \times 100\,, \tag{2}$$

where A_D = desired total attenuation, D_U = unprotected radiation dose, and D_V = dose at which the percent viability of the BM cell is equal to percent viability of active BM necessary for hematopoietic reconstitution (P_R). P_R = percent viability of active BM necessary for reconstitution; V_N = volume necessary for reconstitution (23 to 58 cm^3, size dependent) and V_P = volume of protected active BM.

The Visible Human Data set was employed to calculate tissue attenuation (A_T). The Visible Human Project is the creation of complete, anatomically detailed, 3D representations of the human body (Ackerman et al. 1994; NIH 2012; Spitzer and Whitlock 1998; Spitzer et al. 1996). The data set includes complete transverse and reconstructed longitudinal cryosection images of representative male and female cadavers. This tool, which has been used for the construction of accurate digital phantoms in several radiodosimetry studies, allowed the measurement of the thickness and determination of the overall radiodensity of tissues surrounding active BM sites (Caon 2004; Xu et al. 2000). Using cross sectional data from the Visible Human pelvic area (Fig. 1a), an anatomically accurate digital phantom was created (Fig. 1b–d) allowing the mapping of the tissue type and thickness present between the selected BM centers and radiation entry points for hundreds of points around the waist area. Inputting this data into the following formula arrived at the true tissue attenuation at a given point:

$$A_T(x,y,z) = b \times e^{-\mu x}\,, \tag{3}$$

where A_T = tissue attenuation; b = build-up factor for one energy at tissue thickness x; μ = linear attenuation coefficient in cm^{-1}; x = tissue thickness between BM and body surface point (x,y,z) in cm. A_T and A_D then allowed the calculation of the required attenuation (A_R) of the shielding at any given point (eqn 4) and subsequently to the shielding thickness at any point (eqn 5):

$$A_R(x,y,z) = \frac{A_D}{A_T} \tag{4}$$

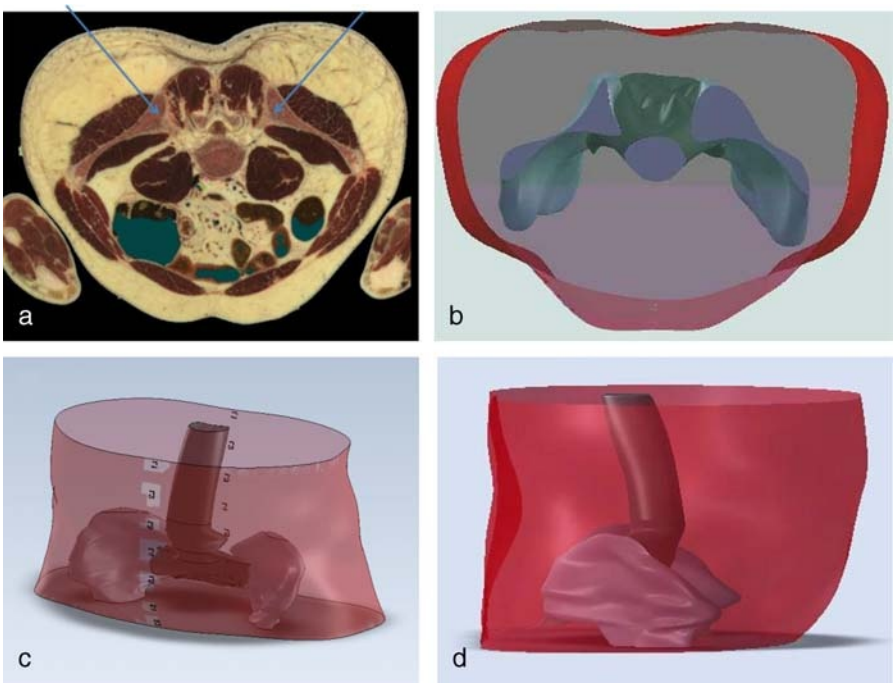

Fig 1. Building an anatomically accurate digital phantom using The Visible Human Project. a. Traverse section through the pelvis of the Visible Human cadaver (Z axis = upper L5). The iliac crests are marked with arrows. b–d. StemRad's digitalization of the Visible Human data set. In b, a top view corresponding to a is shown. In c and d a full 3D reconstruction of the torso with bone marrow is shown in perspective and side views, respectively.

$$Thickness\,(x,y,z) = \frac{\ln(b \times A_R)}{\mu}\ . \qquad (5)$$

This led to a belt-like radiation protection selective shielding device with variable thickness, using only the minimal amount of shielding material needed (Fig. 2). This selective shielding device in combination with the body's tissue is configured to provide a substantially uniform fourfold total radiation attenuation (^{137}Cs) to 300 cm^3 of active BM in the posterior pelvis and lesser degrees of protection to an additional ~300 cm^3 of active BM. The shielding material of the selective shielding device is provided in the form of multiple uniquely shaped 1-mm sheets of virgin lead, chosen for their mass efficiency in shielding gamma radiation (Jaeger et al. 1968), which are layered upon each other forming a shielding device of a topography inversely related to the thickness and density of the tissue present between the selective shielding device and the protected active BM in the iliac crest.

Experimental setup and configuration

Irradiations were performed at Pacific Northwest National Laboratory (PNNL) on a male phantom that would result in an approximate simulation of radiation exposure of an individual to a cloud-like source of ^{137}Cs. This source-phantom irradiation geometry could also simulate the radiation dose to an individual walking and turning numerous times in an enclosed environment that contains multiple sources at various heights relative to the individual. These irradiations were conducted with the phantom both shielded and unshielded with embedded dosimetry to measure changes in absorbed doses at internal points of interest (active BM concentrations and abdominal organs) resulting from the selective shielding device.

RANDO phantom geometry

The male RANDO® phantom used for the test irradiations at PNNL, Richland, WA, was manufactured by Alderson Corporation (Long Beach, CA, USA). The RANDO® man represents a 175-cm-tall and 73.5-kg male figure without limbs. RANDO® is constructed with a real human skeleton that is cast inside soft tissue-simulating material. The phantom is constructed of horizontal slices of 2.54 cm thickness to allow access to the thermoluminescent dosimeter (TLD) cavities. Each slice contains approximately 40 of these cavities, each 4.8 mm diameter in a 3.5-cm grid pattern (Fig. 3a). Forty additional TLD cavities were added to the RANDO® at specified locations to measure the absorbed dose to the active BM tissue in the lower spine and pelvis. ImageJ software (Schneider et al. 2012) was used to construct 3D models of the red bone marrow within slices 22–32 of the RANDO phantom. The 2D images of each slice face were loaded into the segmentation editor of ImageJ as image stacks and the red BM regions were

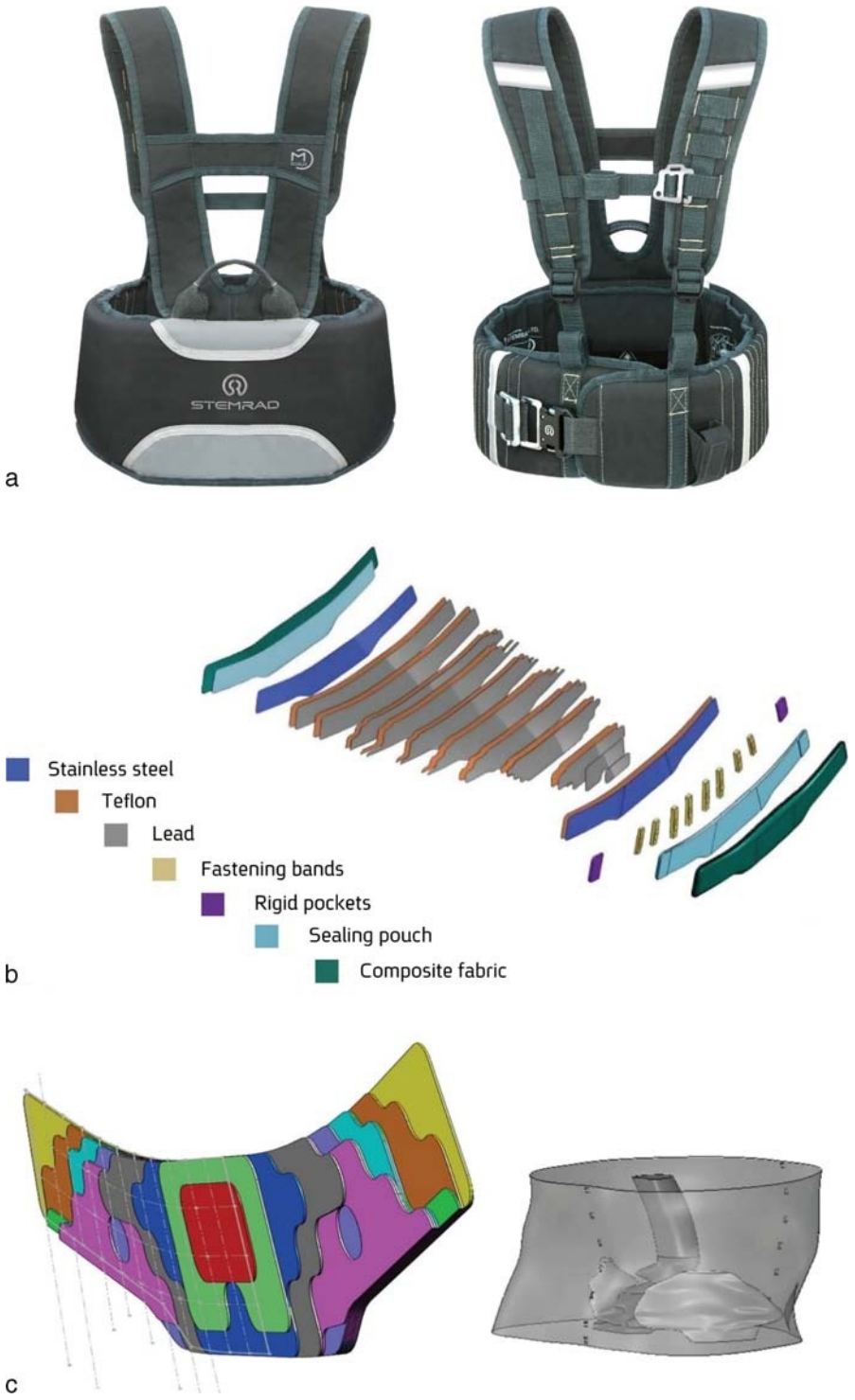

Fig 2. Shielding Device a. The outer shell of the shielding device is designed for maximal comfort and may be worn by use of suspenders. b. The radiation attenuating component of the shielding device is comprised of multiple uniquely shaped 1 mm sheets of virgin lead with friction minimizing dividers placed between them and multiple other structural elements to maintain flexibility and durability. c. The topography of attenuation component matches the anatomy of the underlying BM such that it is of a thickness inversely related to the thickness and density of the tissue present between the device and the BM, thereby minimizing weight without compromising protection.

highlighted as regions of interest and interpolated to form 3D volumes of the red BM within the RANDO slices. Because of the relative spatial uniformity of the spinal column, the vertebral volumes were assigned one TLD cavity only for each slice (totaling 7 cavities). The remaining 33 cavity locations were then identified by calculating the center of

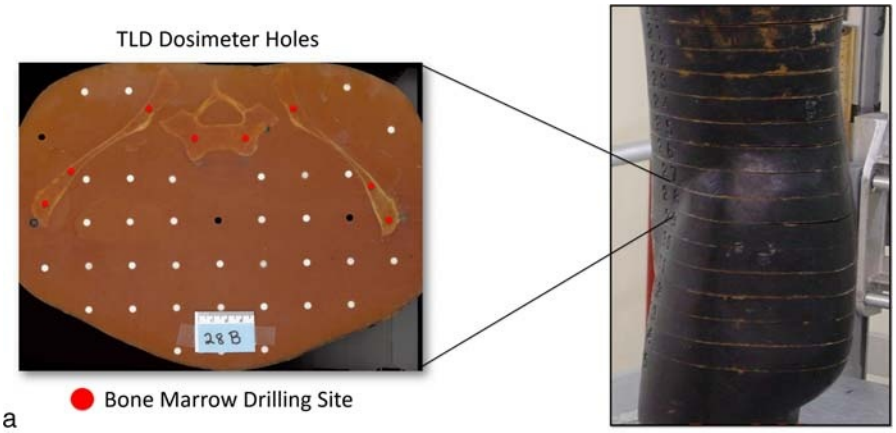

a

TLD Distribution

Tissue/Organ	Number of TLD Cavities	Number of TLDs
Lumbar Spine (RBM)	7	21
Pelvis (RBM)	33	99
Colon	18	54
Small Intestine	32	96
Ovaries	2	6
Total	92	276

b

Fig 3. TLD cavity sites within RANDO phantom slices. a. A sample slice demonstrating TLD sites. Red dots are additional TLD cavities drilled into RANDO in bone marrow concentration sites (left). Location of slice in RANDO from external view is shown (right). b. The distribution of TLDs within RANDO is shown.

masses of 33 equal volumes of the pelvic red bone marrow within these slices. This method allowed the matching of absorbed doses in these cavities to specific masses of red BM within the lower spine and pelvis. These 40 additional cavities were 33 cavities distributed equally in the pelvic BM and seven representing equal volumes of lumbar vertebrae BM. Another 52 TLD cavity locations were used to measure doses to the colon, small intestine, and ovaries. In total, absorbed doses were measured at 92 distinct cavities in the presence vs. in the absence of the selective shielding device using three lithium fluoride TLDs positioned within each of the cavities (Fig. 3b).

Structure and positioning

To ensure precise distances between the source, floor, and RANDO®, a reference point was defined near the middle of the torso at the geometric center on the top of slice 29. The z-axis of rotation was relative to this reference point. The selective shielding device was fit to RANDO® with the posterior of the selective shielding device spanning between slices 24.5 and 33.5. This fit was consistent with the proper donning of the device for ergonomic and shielding of the active BM purposes. Fig. 4 shows the selective shielding device on RANDO®, although the irradiation was done without clothing. The posterior side of the shielding measures 18 cm in height, and the vertical center of this posterior shielding was positioned to be lined up with the reference points in both the RANDO® phantom and the Monte Carlo n-Particle Code (MCNP) simulations, which were also a part of this investigation.

Source and irradiation geometry

An encapsulated ^{137}Cs source consisting of a total of 0.078 inch stainless steel and 0.125 inch aluminum was used. Encasing results in the elimination of the beta particle part of the spectrum associated with the nuclide, and only the gamma spectrum is seen (peaks at 662 keV). To create a realistic fallout setting, the source was shifted in relation to the phantom to five discreet positions (0°, ±22.5° and ±45°) along the Z-axis relative to the reference point, while the phantom itself was rotated at a rate of 1 RPM along the X-Y plane (Fig. 4). Only the source position near the ground (−45°) resulted in measurable ground scatter (approximately 4.5%), and this was taken into consideration. This geometry and photon energy are well within the parameters to provide an approximate whole body uniform irradiation (Bond et al. 1957).

Post-irradiation, the TLDs were extracted. Doses absorbed at bone marrow concentrations, gastrointestinal

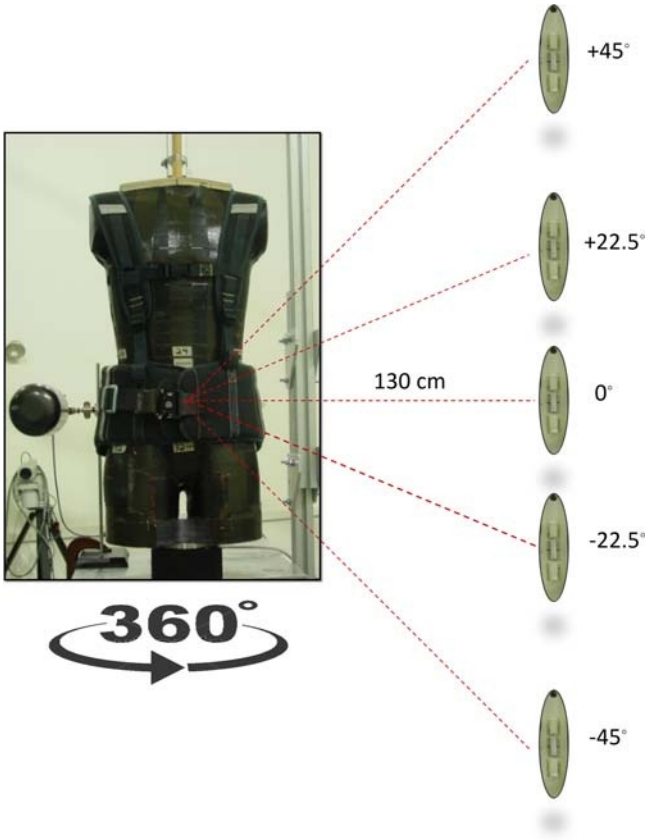

Fig 4. Experimental Set-Up. RANDO phantom embedded with TLDs in bone marrow centers, gastrointestinal tissues, and ovary locations, was employed to measure total integrated dose at specific sites inside the phantom. The phantom was then subjected to irradiation with a 179 GBq ^{137}Cs (0.662 MeV) source (right). To create a realistic fallout setting, the source was shifted in relation to the phantoms to 5 discreet positions (0°, ±22.5° and ±45°) along the Z-axis while the phantom itself was rotated at a rate of 1 RPM along the X-Y plane. Precise source-reference position and angles are shown.

tissues, and ovaries in the presence vs. in the absence of the selective shielding device were determined on a Harshaw 5500 TLD reader. To determine radiation attenuation, the dose recorded in a particular TLD was divided by the ambient dose, arriving at the relative dose. Ambient dose was determined based on the in-air kerma measured by a Capintec Model PR-18 ionization chamber at the position that the central reference point of the phantom occupied during the irradiations. The dose characterization due to the source-phantom geometry as measured by the ionization chamber is depicted in Table 1.

MONTE CARLO N-PARTICLE (MCNP) CODE SIMULATIONS

Simulation of experimental conditions

The experimental conditions were reproduced using the MCNP code and evaluated the ability of the selective shielding device to reduce the dose absorbed in the pelvic and vertebral BM using point sources of ^{137}Cs. A version of the computerized ORNL-MIRD phantom with a modified pelvic and lumbar spine geometry to increase the resolution of absorbed dose to the active BM was used (Eckerman et al. 1996). The phantom was positioned standing on a concrete slab of 30 cm thickness to allow for ground scatter. Twenty point sources were used in a geometry similar to that used in the experimental irradiation; four sources at each of five different heights at 0°, ±22.5° and ±45° vertically (on the z-axis) and rotated in four positions in the x-y plane every 90° relative to the origin (same as ref. point used in the experiment) which is the center of torso cell at the height corresponding to where the L-5 vertebra and sacrum meet.

Simulation of cloud, ground, and mixed source geometries with variable energies

MCNP simulations with more complex source geometries and multiple energies were then used to analyze the selective shielding device's efficacy under conditions of interest to first responders. These source geometries included a cloud source, a planar ground source, and an equal combination of the two. All of these simulations used the same phantom geometry described above complete with concrete slab. In the cloud source simulation, isotropic photons were generated throughout the volume surrounding the phantom, resulting in all possible angles of incidence including above the head and just above the surface of the concrete slab. This represents an early-stage scenario in

Table 1. Angles, distances and dose rates (measured by ionization chamber at reference point) associated with RANDO and ^{137}Cs source.

Source position	Source height off floor (cm)	Source–Slice 29 reference distance (cm)	Source-RANDO Z-axis distance (cm)	mR h^{-1} in AIR (slice 29)	mR in 1.6 h in AIR (slice 29)
+45°	300	184	130	379	606
+22.5°	224	141	130	645	1032
0°	170	130	130	759	1214
−22.5°	116	141	130	645	1032
−45°	40 (~4.5% scatter)	184	130	396	634
	Total exposure: 4.518 R			Total air kerma: 3.967 cGy	

which radioactive material has been released into the air but has little to no accumulation on the ground. In the planar ground source simulation, isotropic photons originated on the surface of the concrete slab at the feet of the phantom representing a 100% ground source. This represents a later stage scenario in which there is no radioactive material present in the air, but it has accumulated on the ground. For the 1:1 Cloud to Ground source, an equal number of photons originated on the ground surface and volume around the phantom, representing an intermediate situation.

At the initial release of fallout, 700 keV (Glasstone and Dolan 1977) is the average photon energy, but this average drops to less than 500 keV within 48 h (Smith 2011). For this reason, the protection provided by the selective shielding device at these energies is also of interest for first responders. Therefore, the cloud, ground, and mixed sources simulations described were repeated using photon energies of 500 keV, 662 keV, and 700 keV.

RESULTS

Experimental results

Experimental layout and results are summarized in Table 2. The three TLDs in each phantom cavity were averaged to determine the absorbed dose at each discrete location. These mean absorbed dose values were then mapped to all cavities encompassing the entire tissue or organ which they represented based on their anatomical positions inside the phantom. Both mean attenuation of dose throughout the organ and peak attenuation points were studied. The peak attenuation is especially relevant to sparing of bone marrow as the survivability of the hematopoietic stem cells is exponentially increased with reduction of dose (Senn and McCulloch 1970). The mean relative absorbed dose of the shielded phantom's BM volumes in the pelvis and lumbar vertebrae divided by the mean relative dose of the unprotected phantom's BM results in a mean belt on/belt off ratio of 0.59 (Table 2). One minus this ratio, 0.41, provides the mean percent reduction in absorbed dose to the protected BM attributed to the selective shielding device (41%). While the shielding provided by the selective shielding device was significant at all pelvic area points studied, it was especially evident in the posterior iliac crest where the peak attenuation was registered. There the authors observed a 58% reduction in absorbed dose to the active BM from the selective shielding device (Table 2). This maximum point of attenuation was used to calculate the protection factor by which the absorbed dose to a critical mass of active BM is reduced by the selective shielding device, resulting in a protection factor of 1/0.42 or 2.4. The mean absorbed dose reduction for other organs in the pelvic region was 34% for the ovaries, 27% for the large intestine, and 26% for the small intestine (Table 2).

MCNP simulations based on experimental conditions

The energy deposition (MeV g^{-1}) reported by F6 tally results for the active BM regions represent absorbed doses, which were compared in the shielded and unshielded geometries. The maximum reduction in absorbed dose was in a region of the sacrum with a 57% reduction compared to the same region in the unshielded phantom, and the mass weighted average of absorbed dose reduction for the active BM sampled in the simulation was 42%. Both values were in good agreement with the maximum and average dose reduction to the BM from the experimental results (58% and 41%, respectively). The protection factor as defined above was 2.3. The absorbed dose reduction to other organs in

Table 2. Summary of experimental conditions and results for the radiation study. The shielding device size, small-tall, matches the waist size and height of the phantom based on manufacturer parameters for the equipment. All shield attenuation percentages are calculated based on ratio of measured absorbed doses from TLD in the cavity sites representing the particular tissues/organs of the shielded and base-line unshielded phantom.

Source type, energy	179 GBq ^{137}Cs, 662 keV
Irradiation Geometry simulating cloud source	Phantom rotated incessantly at 1 RPM with source shifting to 5 discrete locations along Z-axis
Phantom type	RANDO® phantom with a real human skeleton cast inside soft tissue-simulating material
Number of measured sites per phantom	92
Number of TLDs per site	3
Tissues represented by TLD sites	bone marrow, large and small intestines and ovary equivalents
Shielding Device Size	Small–Tall
Maximum shield attenuation to pelvic bone marrow	58%
Average shield attenuation to pelvic bone marrow	41%
Average shield attenuation to large intestine	27%
Average shield attenuation to small intestine	26%
Average shield attenuation to ovary equivalents	34%

the pelvic area was ovaries 29% dose reduction, intestines 30% dose reduction, and the stomach had a 19% dose reduction. The experimental and experimental conditions MCNP simulation results show close agreement, providing validation to the simulation results for the more complex geometries that were not tested experimentally.

MCNP simulations of cloud, ground, and mixed source geometries with variable energies

The protection factors for the cloud, ground, and 1:1 Cloud-Ground sources were calculated at discrete photon energies of 700, 662, and 500 keV and are shown in Table 3, along with the protection factors from the irradiation simulation and experiment. Importantly, all protection factors showed a roughly 2-fold absorbed dose reduction to a critical mass of active BM regardless of source geometry or energy; this exhibits efficacy of the shielding device for all scenarios investigated. Unsurprisingly, the protection factors show an inverse relationship with photon energy. At 662 keV photon energy, the cloud source simulation was most similar to the experimental irradiation and experimental conditions simulation protection factor values, which makes sense as the experimental source geometry was intended to mimic a cloud source irradiation.

In the cloud, 1:1 Cloud-Ground, experimental conditions simulation and experimental geometries, the critical mass of active BM with the greatest reduction in absorbed dose was in the posterior pelvis region; specifically, the iliac crest in the case of the experimental results and sacrum in these MCNP simulation results. However, in the ground source geometry simulations, the high angle of incidence from below the phantom resulted in a shift of protection from the selective shielding device to the critical mass of active BM in the lumbar vertebrae. This results in surprisingly high protection factors for the ground source geometry simulations, and this trend was consistent over all energies investigated.

Table 4 shows the average absorbed dose reduction percentages for the ovaries, intestines, stomach and total active BM from both the experimental irradiation, the MCNP simulation reproducing the experimental source geometry, cloud, ground, and mixed cloud-ground MCNP source geometry simulations with variable photon energies. This data is most applicable to stochastic effects whereas the protection factors in Table 3 are more applicable to deterministic effects.

Table 3. Protection Factors by which the absorbed dose to a critical mass of active BM is reduced by the selective shielding device in all simulation source geometries and the experiment.

Energy (keV)	Cloud MCNP	1:1 Cloud-ground MCNP	Ground MCNP	Experimental conditions MCNP	Experiment
700	2.0	1.6	1.8	—	—
662	2.1	1.7	1.9	2.3	2.4
500	2.5	1.9	2.1	—	—

Table 4. Absorbed dose reduction in percent to specific organs protected by the selective shielding device. All Cloud, Cloud-Ground, and Ground source geometry results are from MCNP simulations.

		Average organ absorbed dose reduction (%)			
Photon energy (keV)	Source geometry	Ovaries	Intestines	Stomach	Total body active BM
662	Experimental	35	26	N/A	19
662	Experimental Conditions MCNP	29	30	19	17
500	Cloud	30	30	21	17
500	1:1 Cloud-Ground	14	20	23	13
500	Ground	1	6	29	6
662	Cloud	29	22	17	15
662	1:1 Cloud-Ground	14	15	20	11
662	Ground	1	6	26	4
700	Cloud	24	22	17	14
700	1:1 Cloud-Ground	11	14	19	11
700	Ground	0	3	24	4

For the total active BM average dose reduction data, only a portion of total tissue in the body has been protected through selective shielding, so the mean reduction in dose has been multiplied by the fraction of protected active bone marrow divided by total active bone marrow.

In the case of the absorbed dose reduction to the intestines in the experiment, the absorbed dose reductions for the colon and small intestine were measured separately as 27.0% and 25.7%, respectively, but were averaged in Table 4 for the sake of comparison to the simulation.

Some trends are evident in Table 4. For any given energy, the transition from cloud to 1:1 Cloud-Ground and then to Ground source shows a decreased mean dose reduction to the ovaries, intestines, and total active BM and an increase in mean dose reduction to the stomach due to its superior position; hence, more protection of the stomach from photons originating below the phantom. Resembling the protection factors, the average organ absorbed dose reduction values have an inverse relationship with photon energy.

Preservation of viable active bone marrow analysis

Using the attenuation conferred by the selective shielding device at each point in the pelvic marrow, the absorbed dose to active BM assuming a dose of 6 Gy BM midline tissue dose (BM-MLTD), corresponding to 8.65 Gy in-air kerma, using a ^{137}Cs source was determined. The dose 6 Gy BM-MLTD was chosen as a high dose point of interest because it is near the $LD_{50/60}$ when antibiotics and transfusion support are provided and nearly twofold higher than the $LD_{50/60}$ of 3.25–4 Gy for those managed without supportive

care (Fujita et al. 1991; Waselenko et al. 2004). To this end, it was assumed that the total amount of active marrow of the phantom was identical to that of the Computerized Anatomical Man (CAM), age corrected for a 25-y-old (1,266 g) (Watchman et al. 2007). The distribution of the active BM in the body was used to determine how much resided in the lumbar spine and pelvic regions (ICRP 2002). Since the TLD cavities were evenly distributed through the pelvic BM volume, the mean absorbed dose of the three TLDs in each of the 33 pelvic cavities was correlated to a precise mass of active BM. The vertebral TLD cavities' mean absorbed doses were also applied to the specific masses of active BM that they represented. Fig. 5 shows the absorbed dose to the active BM histogram based on this analysis; a dramatic shift in absorbed dose to active BM is evident in the presence of the selective shielding device. Based on the human BM radiosensitivity curve (Senn and McCulloch 1970), the precise amount of live active BM that would remain following a whole-body uniform exposure resulting in 6 Gy BM-MLTD in the absence vs. in the presence of the selective shielding device (Fig. 5—red bars) was determined. Adding together the amounts of live active BM gave a total of 6 g for an individual exposed without protection and 41 g for an individual equipped with the selective shielding device. This process of dose extrapolation to 6 Gy BM-MLTD was repeated for the MCNP analysis of the experimental geometry simulation using the shift of absorbed dose to the active BM to determine the amount of viable active BM for the shielded phantom and unshielded cases. The results were similar to that of the experiment with 48 g of viable active BM in the shielded case and 8 g for the unshielded. The unprotected, baseline phantom had similar values for viable active BM only at 3.5 Gy BM-MLTD with 43 g remaining using the experimental data and 45 g remaining using the simulation data.

DISCUSSION

Mitigating effect of the selective shielding device on ARS

HSC transplantation (i.e., bone marrow transplantation) can be a life-saving intervention in cases of exposure to high doses of radiation (Alpen and Baum 1958; Chertkov et al. 1971; Department of Homeland Security 2006; MacVittie 1997; Thomas et al. 1982). The bone marrow quantities used in the current practice of transplantation of irradiated human recipients are, depending on the recipient's weight, between 24 and 61 g of net active bone marrow on average (after deduction of plasma and blood cell

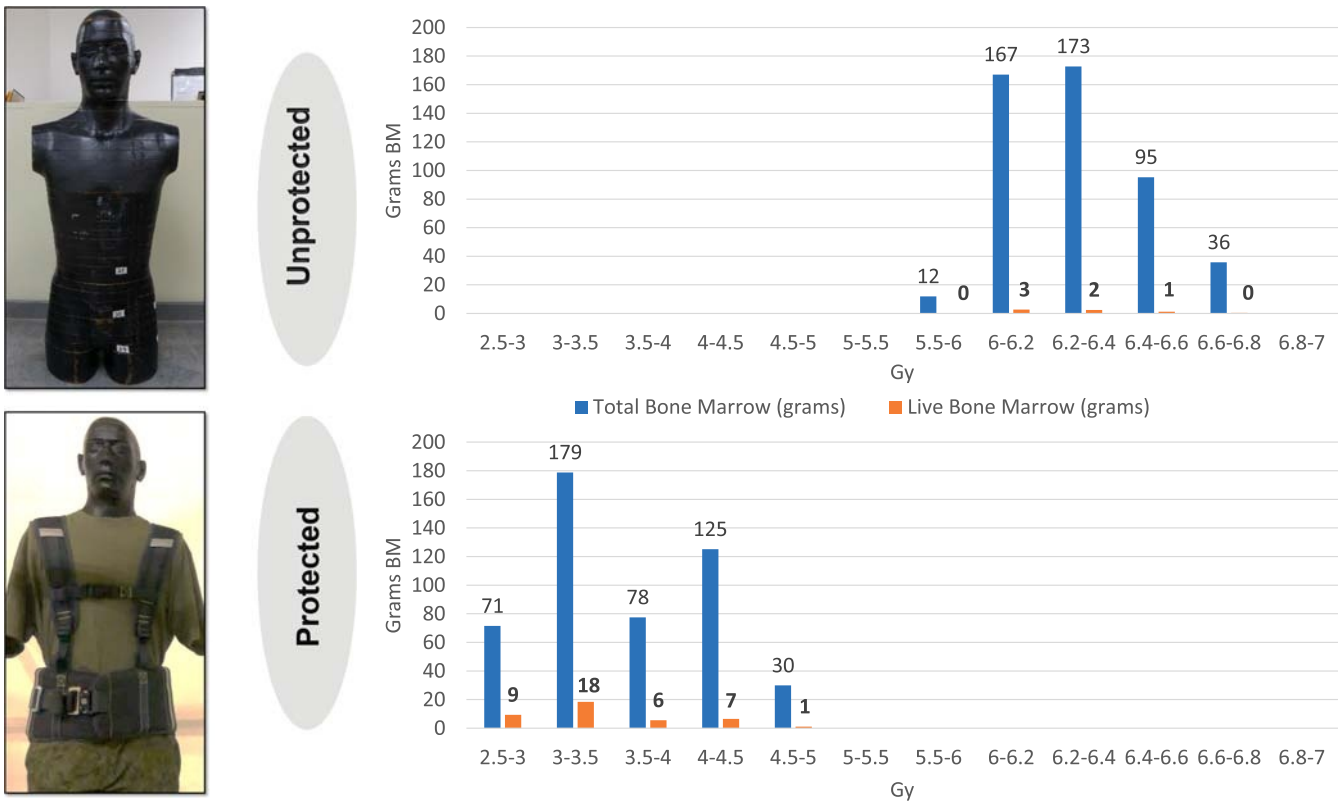

Fig 5. 6 Gy BM- midline tissue dose (corresponding to 8.65 Gy in-air kerma) and resulting live BM quantities (shown in orange). The distribution of absorbed dose to active BM in 50 and 20 cGy dose bins for unprotected and protected individuals is shown.

infiltrates) (Pichardo et al. 2007; National Marrow Donor Program 1993).

By selectively shielding the bone marrow of the lumbar spine and pelvic region from penetrating gamma radiation (this device is not effective in mitigating neutron doses), the shielding device described here is able to preserve in excess of the quantity of active live marrow necessary for the reconstitution of a lethally irradiated average-sized adult even at exposures as high as 6 Gy BM-MLTD (41 g and 48 g for the measurement and the simulation, respectively). This is in sharp contrast to the unshielded results where, beyond 4 Gy BM-MLTD, less than 30 g of viable active BM remained in both the experiment and experimental conditions MCNP simulation. This suggests that the wearing of the selective shielding device during a high dose exposure would have similar benefits to that of a successful bone marrow transplant post-exposure without the difficulties of donor matching in the case of allogeneic transplantation.

The $LD_{50/60}$ of whole-body radiation is between 3.25 Gy and 4 Gy in persons managed without supportive care and 6 to 7 Gy when antibiotics and transfusion support are provided (Fujita et al. 1991; Waselenko et al. 2004). At 3.5 Gy BM-MLTD, the unshielded phantom in the experiment and simulation both showed a similar amount of viable active BM as the shielded case had at 6 Gy BM-MLTD. This suggests that at the approximate $LD_{50/60}$, for persons managed without supportive care, there is a significant shift of a factor of 1.7.

In cases of cytokine treatment, multi-organ dysfunction syndrome (MODS), multi-organ injury (MOI), or multi-organ failure (MOF), the situation is much more complicated to relate the precise levels of survival due to the limited data in this area for humans. However, the literature supports the view that the number of surviving HSC correlates well with mortality in uniformly and nonuniformly irradiated animals (Bond et al. 1967, 1991), so even in these complex cases or at doses beyond 6 Gy BM-MLTD, the larger fraction of viable BM remaining would likely result in reduced mortality at least until such doses where the gastrointestinal syndrome dominates at about 11 Gy (CDC 2012). The selective shielding device described in this work may provide benefits, especially in combination with supportive care and cytokine treatment, in cases of MOI/MOF as damage to the gut, internal bleeding, and infection are all hallmarks of this condition (Bertho et al. 2008; Fliedner et al. 2005; Goans and Flynn 2012; Goans and Wald 2005), which are mitigated to various degrees through dose reduction to the HSC and gastrointestinal system shown here. Additionally, since non-human primate studies of G-CSF use BM sparing to ensure that sufficient numbers of HSC remain after irradiation to be stimulated by G-CSF therapy (Bertho et al. 2005a; MacVittie et al. 2015; Monroy et al. 1988), the use of a selective shielding device may have a synergistic effect with these treatments in humans through the same mechanism.

Not only is this critical mass of viable active BM preserved up to 6 Gy BM-MLTD (corresponding to 8.65 Gy in-air kerma), but the protection factors shown in Table 3 ensure that critical masses of active BM remain viable at all doses below 6 Gy BM-MLTD for all geometries in the energy range investigated (up to 700 keV average photon energy). The protection of large portions of BM combined with a 26% reduction in absorbed dose to the intestines reduce the morbidity and mortality probability associated with ARS.

Radiation-induced nausea and vomiting has been reported in accident victims and radiation treatment patients shortly after irradiation, due to increase of serotonin level (Goans 2002; Goans and Flynn 2012). The increased serotonin then activates the receptors in the chemoreceptor trigger zone in the brain, resulting in nausea and vomiting. While the primary source of serotonin is the enterochromaffin cells of the GI tract (inside of shielded field), it also was found in blood platelets and the central nervous system (outside of shielded field). The selective shielding device is also likely to reduce the symptoms of nausea and vomiting in the prodromal phase of ARS due to the ~20% dose reduction (Table 4) to the enterochromaffin-like cells of the gastrointestinal tract found in the gastric glands of the gastric mucosa beneath the stomach epithelium which are believed to be responsible for these prodromal phase symptoms of ARS (Macia et al. 2011).

Effect of the selective shielding device on radiation-induced cancer

In addition to the mitigation of the hematopoietic subsyndrome of ARS, the selective shielding device may also offer protection against the stochastic effects of radiation exposure. This is accomplished through the absorbed dose reduction provided by the selective shielding device to the organs in the abdominal area, including the ovaries in females, small and large intestine/colon, stomach and total body active bone marrow shown in Table 4. By reducing the absorbed doses to the total active bone marrow, stomach, ovaries, and colon, which are all relatively prone to radiation-induced cancer incidence, the selective shielding device is a valuable tool from an ALARA perspective. The ovaries, stomach, colon, and BM are all weighted heavily by their tissue weighting factors for the calculation of effective dose, and the protection of organs in the abdominal area has been identified as a high priority for radiological protection based on a study of cancer mortality and emergency workers in Japan (Ogino et al. 2016).

Although not related to cancer, it is appropriate to note here that although the male testes are outside of the coverage area of this selective shielding device, the ovaries enjoy

approximately a 34% reduction in absorbed dose (Table 4). This dose reduction to the ovaries may be significant in maintaining fertility at high doses as two to four fractionated doses to the ovaries of 3.6–7.2 Gy has been shown to result in a 97% incidence of sterility in women (Ogilvy-Stuart and Shalet 1993).

CONCLUSION

This novel bone marrow shielding device is capable of securing the survival of a critical volume of active bone marrow and as such may offer dramatic improvements in the survivability of emergency responders, even under extreme radiological scenarios in which prevention of exposure to high doses fails. This device is also effective in reducing the cumulative marrow, ovarian, and colon absorbed doses over the lifetime of personnel if used while performing tasks with potentially abnormal gamma exposures. As such, it may be used to protect professionals in a variety of occupations ranging from gamma radiography and agricultural sterilization to radiological explosive ordinance disposal.

Acknowledgment—The work at PNNL was performed under the Work for Others Program, and any research results that were generated are experimental in nature. Neither the United States Government, nor any agency thereof, nor Battelle Memorial Institute, nor any of their employees, makes any warranty, express or implied, or assumes any legal responsibility for the accuracy, completeness, or usefulness of any information, apparatus, product, or process disclosed, or represents that its use would not infringe privately owned rights. Reference to any specific commercial product, process, or service by its trade name, trademark, manufacturer, or otherwise, does not constitute or imply an endorsement or recommendation by the United States Government or any agency thereof, or by Battelle Memorial Institute. The views and opinions of authors expressed herein do not necessarily state or reflect those of the United States Government or any agency thereof, or by Battelle Memorial Institute, and shall not be used for advertising or product endorsement purposes.

REFERENCES

Ackerman MJ, Spitzer VM, Scherzinger AL, Whitlock DG. The Visible Human data set: an image resource for anatomical visualization. Medinfo 8:1195–1198; 1994.

Alpen EL, Baum SJ. Modification of x radiation lethality by autologous marrow infusion in dogs. Blood 13:1168–1175; 1958.

Barnett DJ, Parker CL, Blodgett DW, Wierzba RK, Links JM. Understanding radiologic and nuclear terrorism as public health threats: preparedness and response perspectives. J Nucl Med 47:1653–1661; 2006.

Beatty PG, Clift RA, Mickelson EM, Nisperos BB, Flournoy N, Martin PJ, Sanders JE, Stewart P, Buckner CD, Storb R, Thomas ED. Marrow transplantation from related donors other than HLA-identical siblings. N Engl J Med 313:765–771; 1985. DOI: 10.1056/NEJM198509263131301.

Bertho JM, Frick J, Prat M, Demarquay C, Dudoignon N, Trompier F, Gorin NC, Thierry D, Gourmelon P. Comparison of autologous cell therapy and granulocyte-colony stimulating factor (G-CSF) injection vs. G-CSF injection alone for the treatment of acute radiation syndrome in a non-human primate modelInt. J Radiat Oncol Biol Phys 63:911–920; 2005a. DOI: 10.1016/j.ijrobp.2005.03.045.

Bertho JM, Prat M, Frick J, Demarquay C, Gaugler MH, Dudoignon N, Clairand I, Chapel A, Gorin NC, Thierry D, Gourmelon P. Application of autologous hematopoietic cell therapy to a nonhuman primate model of heterogeneous high-dose irradiation. Radiat Res 163:557–570; 2005b. DOI: -10.1667/RR3352.

Bertho JM, Roy L, Souidi M, Benderitter M, Gueguen Y, Lataillade JJ, Prat M, Fagot T, De Revel T, Gourmelon P. New biological indicators to evaluate and monitor radiation-induced damage: an accident case report. Radiat Res 169: 543–550; 2008. DOI: 10.1667/RR1259.1.

Bond VP, Carsten AL, Bullis J, Roth SP. Severity of organ injury as a predictor of acute mortality for disparate patterns of absorbed dose distribution. Radiat Res 128:S9–S11; 1991. DOI: 10.2307/3577995.

Bond VP, Cronkite EP, Sondhaus CA, Imirie G, Robertson JS, Borg DC. The influence of exposure geometry on the pattern of radiation dose delivered to large animal phantoms. Radiat Res 6:554–572; 1957. DOI: 10.2307/3570453.

Bond VP, Robinson CV. A mortality determinant in nonuniform exposures of the mammal. Radiat Res 7(Suppl):265–275; 1967. DOI: 10.2307/3583720.

Caon M. Voxel-based computational models of real human anatomy: a review. Radiat Environ Biophys 42:229–235; 2004. DOI: 10.1007/s00411-003-0221-8.

Centers for Disease Control and Prevention. Acute radiation syndrome: fact sheet for physicians [online]. 2012. Available at ***https://emergency.cdc.gov/radiation/arsphysicianfactsheet.asp***. Accessed 23 December 2016.

Chertkov JL, Sukyasyan GV, Novikova MN, Nemenova NM, Kotlyarov AM, Malanina VN, Udalov GA, Semenov LF. Autologous bone marrow transplantation in irradiated baboons. Radiat Res 46:129–143; 1971. DOI: 10.2307/3573109.

Cole LJ, Haire HM, Alpen EL. Partial shielding of dogs: effectiveness of small external epicondylar lead cuffs against lethal x-radiation. Radiat Res 32:54–63; 1967. DOI: 10.2307/3572306.

Dainiak N. Hematologic consequences of exposure to ionizing radiation. Exp Hematol 30:513–528; 2002. DOI: 10.1016/S0301-472X(02)00802-0.

Department of Homeland Security. National planning scenarios [online]. 2006. Available at ***https://info.publicintelligence.net/DHS%20-%20National%20Planning%20Scenarios%20March%202006.pdf***. Accessed 1 January 2017.

Eckerman KF, Cristy M, Ryman JC. The ORNL mathematical phantom series, informal paper. Oak Ridge National Laboratory: Oak Ridge, TN; 1996. Available at ***http://homer.hsr.ornl.gov/VLab/mird2.pdf***. Accessed 1 March 2015.

Fliedner TM, Dorr HD, Meineke V. Multi-organ involvement as a pathogenetic principle of the radiation syndromes: a study involving 110 case histories documented in SEARCH and classified as the bases of haematopoietic indicators of effect. Br Instit Radiol 1:1–8; 2005.

Fujita S, Kato H, Schull WJ. The LD50 associated with exposure to the atomic bombing of Hiroshima and Nagasaki. J Radiat Res 32(Suppl):154–161; 1991. DOI: 10.1269/jrr.32.SUPPLEMENT_154.

Glasstone S, Dolan P. The Effects of Nuclear Weapons, 3rd ed. Washington, DC: U.S. Government Printing Office. 1977.

Goans RE, Wald N. Radiation accidents with multi-organ failure in the United States. Br Instit Radiol 1:41–46; 2005.

Goans R, Flynn D. Acute radiation syndrome in humans. In: Medical consequences of radiological and nuclear weapons. Falls Church: Office of The Surgeon General United States Army; 17–38; 2012.

Goans R. Clinical care of the radiation-accident patient: patient presentation, assessment, and initial diagnosis. In: Ricks R, Berger M, O'Hara F, eds. The medical basis for radiation

accident preparedness: the clinical care of victims. Boca Raton, FL: CRC Press; 11–22; 2002.
Goldman JM, Apperley JF, Jones L, Marcus R, Goolden AW, Batchelor R, Hale G, Waldmann H, Reid CD, Hows J, Gordon-Smith E. Bone marrow transplantation for patients with chronic myeloid leukemia. N Engl J Med 314:202–207; 1986. DOI: 10.1056/NEJM198601233140403.
Greenberger JS, Epperly M. Bone marrow-derived stem cells and radiation response. Semin Radiat Oncol 19:133–139; 2009. DOI: 10.1016/j.semradonc.2008.11.006.
Hansen JA, Petersdorf EW, Lin MT, Wang S, Chien JW, Storer B, Martin PJ. Genetics of allogeneic hematopoietic cell transplantation. Role of HLA matching, functional variation in immune response genes. Immunol Res 41:56–78; 2008. DOI: 10.1007/s12026-007-0043-x.
International Commission on Radiological Protection. Basic anatomical and physiological data for use in radiological protection reference values. Oxford: Pergamon Press; ICRP Publication 89; Ann. ICRP; 32(3–4);2002.
Jacobson LO, Simmons EL, Marks EK, Eldredge JH. Recovery from radiation injury. Science 113:510–511; 1951. DOI: 10.1126/science.113.2940.510.
Jaeger RG, Blizard EP, Chilton AB, Grotenhuis M, Hoenig A. Engineering compendium on radiation shielding, prepared by numerous specialists. New York: Springer-Verlag; 1968.
Macia IGM, Lucas Calduch A, Lopez EC. Radiobiology of the acute radiation syndrome. Rep Pract Oncol Radiother 16:123–130; 2011. DOI: 10.1016/j.rpor.2011.06.001.
MacVittie TJ, Bennett AW, Farese AM, Taylor-Howell C, Smith CP, Gibbs AM, Prado K, Jackson W III. The effect of radiation dose and variation in Neupogen® initiation schedule on the mitigation of myelosuppression during the concomitant GI-ARS and H-ARS in a nonhuman primate model of high-dose exposure with marrow sparing. Health Phys 109:427–439; 2015. DOI: 10.1097/HP.0000000000000350.
MacVittie TJ. Commentary: therapy of radiation injury. Stem Cells 15(S1):263–268; 1997. DOI: 10.1002/stem.5530150735.
Milstein O, Levitt D, Tikochinsky Y, Zur E, Zur E. Radiation protection device and methods thereof. US Patent 20150004131, filed 14 Nov 2012. Available at ***www.google.com/patents/US20150004131***. Accessed 17 March 2017.
Monroy RL, Skelly RR, Taylor P, Dubois A, Donahue RE, MacVittie TJ. Recovery from severe hematopoietic suppression using recombinant human granulocyte-macrophage colony-stimulating factor. Exp Hematol 16:344–348; 1988.
National Institutes of Health. The visible human project [online]. 2012. Available at ***www.nlm.nih.gov/research/visible/visible_human.html***. Accessed 11 August 2012.
National Marrow Donor Program Standards Committee. Standards of the national marrow donor program. Transfusion 33:172–180; 1993.
Ogilvy-Stuart AL, Shalet SM. Effect of radiation on the human reproductive system. Environ Health Perspect 101(Suppl 2):109; 1993. DOI: 10.2307/3431383.
Ogino H, Fujimichi Y, Sasaki M, Hamada N, Iwasaki T, Yoshida K, Hattori T. Quantitative assessment of provability of radiation-related cancers considering unavoidable existence of unadjusted risk factors. J Radiol Prot 36:865; 2016. DOI: 10.1088/0952-4746/36/4/865.
Organisation for Economic Co-operation and Development–Nuclear Energy Agency, Committee on Radiation Protection and Public Health. Occupational radiation protection in severe accident management [online]. 2015. Available at ***www.oecd-nea.org/rp/docs/2014/crpph-r2014-5.pdf***. Accessed 29 January 2017.
Pearce ML, Greenfield MA, Valentine WN. Studies on the radiosensitivity of bone marrow. Blood 7:207–213; 1952.
Pichardo JC, Trindade AA, Brindle JM, Bolch WE. Method for estimating skeletal spongiosa volume and active marrow mass in the adult male and adult female. J Nucl Med 48:1880–1888; 2007. DOI: 10.2967/jnumed.107.044354.
Schneider CA, Rasband WS, Eliceiri KW. NIH image to image: 25 years of image analysis. Nat Meth 9:671–675; 2012. DOI: 10.1038/nmeth.2089.
Senn JS, McCulloch EA. Radiation sensitivity of human bone marrow cells measured by a cell culture method. Blood 35:56–60; 1970.
Smith JM. Source normalization constants for ground distributed fallout fields. Wright-Patterson Air Force Base, OH: Air Force Institute of Technology; 2011. Thesis.
Spitzer V, Ackerman MJ, Scherzinger AL, Whitlock D. The visible human male: a technical report. J Am Med Inform Assoc 3:118–130; 1996. DOI: 10.1136/jamia.1996.96236280.
Spitzer VM, Whitlock DG. The visible human dataset: the anatomical platform for human simulation. Anat Rec 253:49–57; 1998. DOI: 10.1002/(SICI)1097-0185(199804)253:2%3C49:AID-AR8%3E3.0.CO;2-9.
Stearner SP, Christian EJ, Brues AM. Modification of the radiation syndrome in the chick by partial body shielding. Radiat Res 1:270–281; 1954. DOI: 10.2307/3570372.
Stone HB, Coleman CN, Anscher MS, McBride WH. Effects of radiation on normal tissue: consequences and mechanisms. Lancet Oncol 4:529–536; 2003. DOI: 10.1016/S1470-2045(03)01191-4.
Thomas ED, Clift RA, Hersman J, Sanders JE, Stewart P, Buckner CD, Fefer A, McGuffin R, Smith JW, Storb R. Marrow transplantation for acute nonlymphoblastic leukemia in first remission using fractionated or single-dose irradiation. Int J Radiat Oncol Biol Phys 8:817–821; 1982. DOI: 10.1016/0360-3016(82)90083-9.
Thomas ED, Storb R, Clift RA, Fefer A, Johnson FL, Neiman PE, Lerner KG, Glucksberg H, Buckner CD. Bone-marrow transplantation (first of two parts). N Engl J Med 292:832–843; 1975a. DOI: 10.1056/NEJM197504172921605.
Thomas ED, Storb R, Clift RA, Fefer A, Johnson FL, Neiman PE, Lerner KG, Glucksberg H, Buckner CD. Bone-marrow transplantation (second of two parts). N Engl J Med 292:895–902; 1975b. DOI: 10.1056/NEJM197504242921706.
United Nations Scientific Committee on the Effects of Atomic Radiation. Sources and effects of ionizing radiation UNSCEAR 2000 Report to the General Assembly with Scientific Annexes. New York: United Nations; UNSCEAR 2000; Volume II; Ann J: 451–566; 2000.
United Nations Scientific Committee on the Effects of Atomic Radiation. Sources and effects of ionizing radiation UNSCEAR 2008 Report to the General Assembly with Scientific Annexes. New York: United Nations; UNSCEAR 2008, Volume II; Ann C, D, E; 2011.
Valentine WN, Pearce ML, Lawrence JS. Studies on the radiosensitivity of bone marrow. II. The effect of large, repeated whole body irradiation exposure on hematopoiesis. Blood 7:14–19; 1952.
Valentine WN, Pearce ML. Studies on the radiosensitivity of bone marrow I. The relative sensitivity of erythroid and myeloid elements. Blood 7:1–13; 1952.
Van Bekkum DW, Schotman E. Protection from haemopoietic death by shielding versus grafting of bone-marrow. Int J Radiat Biol Relat Stud Phys Chem Med 25:361–372; 1974. DOI: 10.1080/09553007414550431.
Van Bekkum DW. Radiation sensitivity of the hemopoietic stem cell. Radiat Res 128:S4–S8; 1991. DOI: 10.2307/3577994.

Wang LD, Wagers AJ. Dynamic niches in the origination and differentiation of haematopoietic stem cells. Nat Rev Mol Cell Biol 12:643–655; 2011. DOI: 10.1038/nrm3245.

Waselenko JK, MacVittie TJ, Blakely WF, Pesik N, Wiley AL, Dickerson WE, Tsu H, Confer DL, Coleman CN, Seed T, Lowry P. Medical management of the acute radiation syndrome: recommendations of the Strategic National Stockpile Radiation Working Group. Ann Intern Med 140: 1037–1051; 2004. DOI: 10.7326/0003-4819-140-12-200406150-00015.

Watchman CJ, Hasenauer D, Bolch WE. Derivation of site-specific skeletal masses within the current ICRP age series. Phys Med Biol 52:3133–3150; 2007. DOI: 10.1088/0031-9155/52/11/014.

Weinstock DM, Case C, Bader JL, Chao NJ, Coleman CN, Hatchett RJ, Weisdorf DJ, Confer DL. Radiologic and nuclear events: contingency planning for hematologists/oncologists. Blood 111:5440–5445; 2008.

White DR, Woodard HQ, Hammond SM. Average soft-tissue and bone models for use in radiation-dosimetry. Br J Radiol 60: 907–913; 1987. DOI: 10.1259/0007-1285-60-717-907.

Xu XG, Chao TC, Bozkurt A. VIP-Man: An image-based whole-body adult male model constructed from color photographs of the Visible Human Project for multi-particle Monte Carlo calculations. Health Phys 78:476–486; 2000. DOI: 10.1097/00004032-200005000-00003.

■■